Article

# Non-fullerene acceptor photostability and its impact on organic solar cell lifetime

Andrew J. Clarke, Joel Luke, Rico Meitzner, ..., Wing C. Tsoi, Ji-Seon Kim, Zhe Li

w.c.tsoi@swansea.ac.uk (W.C.T.)
ji-seon.kim@imperial.ac.uk (J.-S.K.)
zhe.li@qmul.ac.uk (Z.L.)

Highlights

Excellent photostability of O-IDTBR and EH-IDTBR results in good device stability

ITIC and ITIC-M have poorer photostability, resulting in reduced device lifetimes

Raman spectroscopy reveals twisting and breakage of ITIC upon illumination in $N_2$

Vinylene linkage between the core and the end groups is a weak point of ITIC and ITIC-M

Clarke et al. find that ITIC and ITIC-M can twist upon illumination in inert conditions, leading to eventual bond breakage and poor device stability. In contrast, O-IDTBR and EH-IDTBR devices show excellent stability. These findings provide insights that could aid with the design of more photostable acceptors.

**Cell Reports**
**Physical Science**

## Article

# Non-fullerene acceptor photostability and its impact on organic solar cell lifetime

Andrew J. Clarke,[1,11] Joel Luke,[2,11] Rico Meitzner,[3] Jiaying Wu,[4] Yuming Wang,[5] Harrison K.H. Lee,[1] Emily M. Speller,[1] Helen Bristow,[6] Hyojung Cha,[4] Michael J. Newman,[1] Katherine Hooper,[1] Alex Evans,[7] Feng Gao,[5] Harald Hoppe,[3] Iain McCulloch,[6,8] Ulrich S. Schubert,[3,9] Trystan M. Watson,[1] James R. Durrant,[1,4] Wing C. Tsoi,[1,*] Ji-Seon Kim,[2,*] and Zhe Li[10,12,*]

## SUMMARY

**The development of non-fullerene acceptors (NFAs) has facilitated the realization of efficient organic solar cells (OSCs) with minimal burn-in losses and excellent long-term stability. However, the role of NFA molecular structures on device stability remains unclear, limiting commercialization of NFA-based OSCs. Herein, the photostability of 10 OSC devices, fabricated with various NFAs (O-IDTBR, EH-IDTBR, ITIC, and ITIC-M) blended with donor polymers (PTB7-Th, PffBT4T-2OD, and PBDB-T), is investigated. O-IDTBR and EH-IDTBR form highly stable devices with all three polymers, whereas ITIC and ITIC-M devices suffer from burn-in losses and long-term degradation. Conformational instability is found to be responsible for the poor photostability of ITIC and ITIC-M, resulting in poor device stability. Twisting and potential breakage of the chemical bond that links the end group to the main backbone of ITIC and ITIC-M molecules causes undesirable conformational changes. Potential strategies to overcome such detrimental photo-induced conformational changes in NFAs are proposed.**

## INTRODUCTION

In recent years, the rapid development of non-fullerene acceptors (NFAs) has led to significant improvements in the performance of organic photovoltaics,[1–9] with power conversion efficiencies (PCEs) reaching more than 18% for single-junction binary devices.[10] In comparison to their fullerene counterparts, NFAs offer several key advantages. The ease of adaption of their chemical structures enables a high degree of tunability in their optoelectronic properties. By tuning the band gap, the absorption region can be shifted into the UV, visible, or infra-red regions to target different applications (e.g., for semi-transparent solar cells[11] or indoor light harvesting[12,13]). In addition, through optimization of their molecular orbital energetics, high open-circuit voltages can be attained with minimal voltage losses.[14] It is also foreseen that NFAs may offer simpler synthetic pathways that have the potential to reduce fabrication costs.[3,15]

Organic solar cells (OSCs) are achieving the efficiencies required for commercial viability. However, device stability requires further improvement to make them a competitive next-generation photovoltaic (PV) technology. OSCs typically suffer from rapid degradation under light exposure, induced by different mechanisms depending on the atmosphere.[16–19] Under ambient conditions, there is rapid degradation that has been linked with the degradation of donor polymers[20–23] and, more

[1]SPECIFIC, College of Engineering, Swansea University, Bay Campus, Swansea SA1 8EN, UK

[2]Department of Physics and Centre for Processable Electronics, Imperial College London, London SW7 2AZ, UK

[3]Center for Energy and Environmental Chemistry Jena (CEEC Jena), Friedrich Schiller University Jena, Philosophenweg 7, 07743 Jena, Germany

[4]Department of Chemistry and Centre for Processable Electronics, Imperial College London, London W12 0BZ, UK

[5]Division of Biomolecular and Organic Electronics, Linköping University, 581 83 Linköping, Sweden

[6]Department of Chemistry, Chemistry Research Laboratory, University of Oxford, Oxford OX1 3TA, UK

[7]School of Engineering, Cardiff University, Queen's Buildings, The Parade, Cardiff CF24 3AA, UK

[8]KAUST Solar Center (KSC), King Abdullah University of Science and Technology (KAUST), Thuwal 23955-6900, Saudi Arabia

[9]Laboratory of Organic and Macromolecular Chemistry (IOMC), Friedrich Schiller University Jena, Humboldtstr. 10, 07743 Jena, Germany

[10]School of Engineering, Queen Mary University of London, Mile End Road, London E1 4NS, UK

[11]These authors contributed equally

[12]Lead contact

*Correspondence:
w.c.tsoi@swansea.ac.uk (W.C.T.),
ji-seon.kim@imperial.ac.uk (J.-S.K.),
zhe.li@qmul.ac.uk (Z.L.)
https://doi.org/10.1016/j.xcrp.2021.100498

recently, photooxidation of acceptors.[24–28] Illumination under inert atmospheres can also induce a rapid loss of solar cell performance, resulting in a reduction in efficiency of ~10%–30% within the first tens to hundreds of hours (often called burn-in), followed by a more gradual loss over the next thousands of hours. Because a substantial proportion of device performance can be lost through this initial rapid burn-in process, significant research efforts have been dedicated to unraveling its origins. For example, photo-induced fullerene dimerization has been identified as a major degradation mechanism for polymer:$PC_{61}BM$ OSCs, leading to loss of short-circuit current ($J_{SC}$) during illumination.[29] We and others have identified the formation of disordered states, leading to increased charge traps and voltage losses upon photodegradation.[30,31] Morphological degradation caused by inadvertent heating during illumination was also found to cause a rapid loss in $J_{SC}$ because of thermodynamically driven demixing of intermixed amorphous regions of the bulk heterojunction.[32–35] Encouragingly, the rapid development of NFAs allows the burn-in degradation of some OSC systems to be effectively addressed. For example, multiple NFA-based OSC systems were found to exhibit minimal burn-in losses, and extrapolated OSC lifetimes of more than 10 years have been demonstrated.[30,36,37] Despite intensive mechanistic studies into this topic, the origins of burn-in are debated. The various degradation mechanisms identified suggest multiple origins that strongly depend on the material system being investigated. However, to date, few studies have been dedicated to understanding how burn-in is influenced by the choice of donor and acceptor components of the active layer. Despite some NFA-based OSCs demonstrating minimal burn-in and good lifetimes, there remains a lack of fundamental understanding of the generality of this improved photostability to other classes of NFAs and donor polymers, especially in terms of the underlying degradation mechanisms and hence the molecular design rules for improving lifetimes of NFA-based OSCs.

To date, the IDTBR[2] and ITIC[5–8,38] families have been established among the most promising NFAs, achieving OSC efficiencies of more than 12%[39] and 14%,[40] respectively. For IDTBR-based NFAs, burn-in free devices have been demonstrated for some systems,[30,34,36] but the generality of this behavior to other systems requires further study. The photostability of ITIC-based acceptors in inert conditions is comparatively less clear, and it seems that several factors can affect device photostability. Some studies have reported that ITIC-based materials may be chemically incompatible with commonly used transport layers.[41,42] Another study demonstrated extrapolated operational device lifetimes of up to 10 years for some ITIC derivatives when used with PBDB-T, although these devices still suffered from a small burn-in loss.[37] This study also showed device stability to strongly depended on the end groups and side chains of the ITIC-based acceptors, suggesting that further stability enhancements are possible by optimization of the material design of NFAs at a molecular level.[37] Du et al.[43] also highlighted the importance of initial morphology on device stability for polymer:ITIC-4F-based devices, with performance deterioration being linked with polymer reorganization and diffusion-limited aggregation of NFAs.

Herein, we report an in-depth investigation of the photostability of OSCs based on several popular NFAs, namely, O-IDTBR, EH-IDTBR, ITIC, and ITIC-M. These acceptors are blended with a range of benchmark donor polymers with varying energetics and crystallinity—PTB7-Th, PffBT4T-2OD, and PBDB-T—to give a range of photoactive layers.[7,44–47] OSCs are fabricated and their photostability is systematically tested under continuous white LED illumination in an inert atmosphere. The photostability of the investigated systems is found to be highly dependent on the choice of

## Cell Reports
# Physical Science
## Article

**CellPress**
OPEN ACCESS

NFA but relatively insensitive to the choice of donor polymer. Devices using NFAs from the IDTBR family suffer minimal burn-in across all investigated polymers, whereas all devices using ITIC-based NFAs show more severe burn-in and continuous long-term degradation. Using advanced characterization measurements, we find that ITIC and ITIC-M are susceptible to photo-induced chemical degradation. This leads to decreased optical absorption and increased charge trapping, resulting in poor device stability. Such behavior is not observed for O-IDTBR or EH-IDTBR, correlating with the superior stability of these devices. This work represents the first systematic study to address the generality of burn-in behavior in polymer:NFA OSCs. In addition, it highlights the importance of NFA molecular design as a key strategy to improve the photostability of fullerene-free OSCs.

## RESULTS

### Device characterization

Three donor polymers (PTB7-Th, PffBT4T-2OD, and PBDB-T)[44–46] and four NFAs (O-IDTBR, EH-IDTBR, ITIC, and ITIC-M)[2,5,7] are investigated in this work. The chemical structures of these materials are shown in Figure 1, and the full chemical names are provided in Note S1. All binary donor:acceptor combinations were investigated, except for PffBT4T-2OD:ITIC and PffBT4T-2OD:ITIC-M due to the poor initial performance of these systems. The details of active-layer preparation and deposition can be found in the Table S1. To monitor performance during continuous photoexcitation, devices were placed into a nitrogen-filled environmental chamber and illuminated with a 1 sun equivalent intensity white LED array (spectrum shown in Figure S1). The evolution of the photovoltaic parameters during continuous photoexcitation is shown in Figure 2.

All O-IDTBR- and EH-IDTBR-based OSCs exhibit superior photostability upon 120 h of light soaking, undergoing negligible degradation across all photovoltaic parameters. In contrast, the ITIC- and ITIC-M-based OSCs exhibit a more significant loss in device performance, losing up to ~30% of their initial performance within the first 24 h of illumination. This is followed by more gradual degradation, primarily caused by a continuous loss of fill factor (FF) and $J_{SC}$. Remarkably, degradation strongly depends on the choice of NFA yet is relatively insensitive to the choice of donor polymer across all investigated blends.

To investigate the origin of the strong dependence of photostability on the choice of electron acceptor, further characterization was conducted, with PTB7-Th as a common donor polymer. PTB7-Th was selected because of the good performance achieved when blended with all investigated NFAs (Table S2). Although PBDB-T:ITIC and PBDB-T:ITIC-M devices use 1,8-diiodooctane (DIO) during fabrication, the corresponding PTB7-Th devices do not. This excludes DIO-related stability issues[48–51] from being solely responsible for the poor device stability of the ITIC and ITIC-M devices.

The formation of additional sub-band tail states (also known as shallow trap states) has been previously reported during burn-in for other OSC blends.[30,31,52,53] To probe the impact of prolonged continuous photoexcitation on the transport and recombination kinetics of charge carriers and tail-state configurations, transient photovoltage (TPV) and charge extraction (CE) measurements were performed. Devices were measured before and after 24 h of illumination (Figure 3), covering the burn-in period.

As shown in Figure 3A, PTB7-Th:O-IDTBR and PTB7-Th:EH-IDTBR OSCs exhibit no noticeable change in charge carrier density (measured as a function of open-circuit
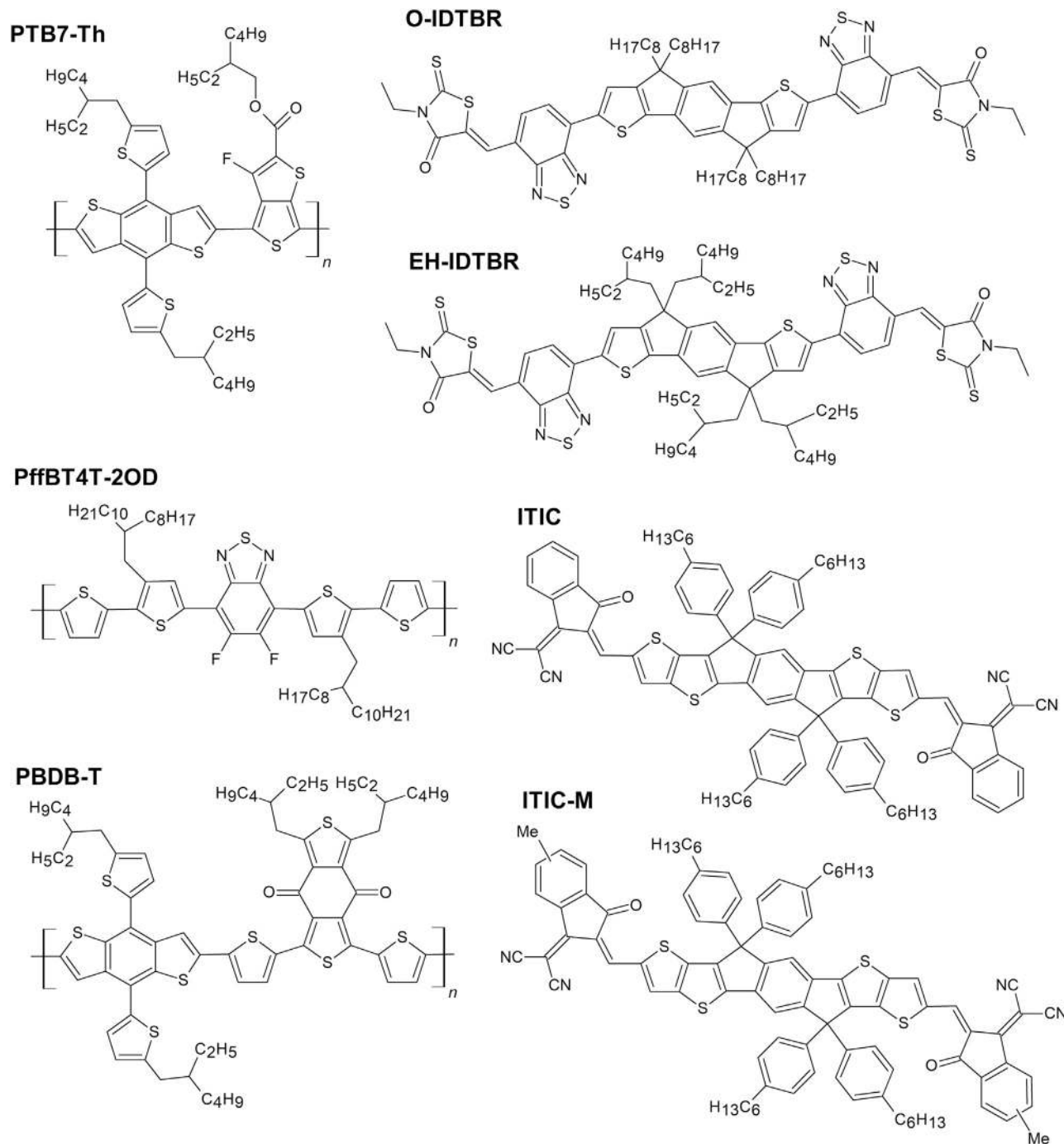
**Figure 1. Schematic representation of the chemical structures of the donor polymers and non-fullerene acceptors used in this work**

Chemical structures of the studied donor polymers (PTB7-Th, PBDB-T, and PffBT4T-2OD) and non-fullerene acceptors (O-IDTBR, EH-IDTBR, ITIC, and ITIC-M).

voltage, $V_{OC}$) upon degradation, whereas a clear increase is seen for PTB7-Th:ITIC and PTB7-Th:ITIC-M OSCs. This increased charge carrier density is assigned to the additional formation of shallow sub-band tail states, as observed in our previous studies.[30] Notably, no clear change in the slope of charge carrier density is seen, suggesting negligible changes in the distribution of the sub-band tail states upon
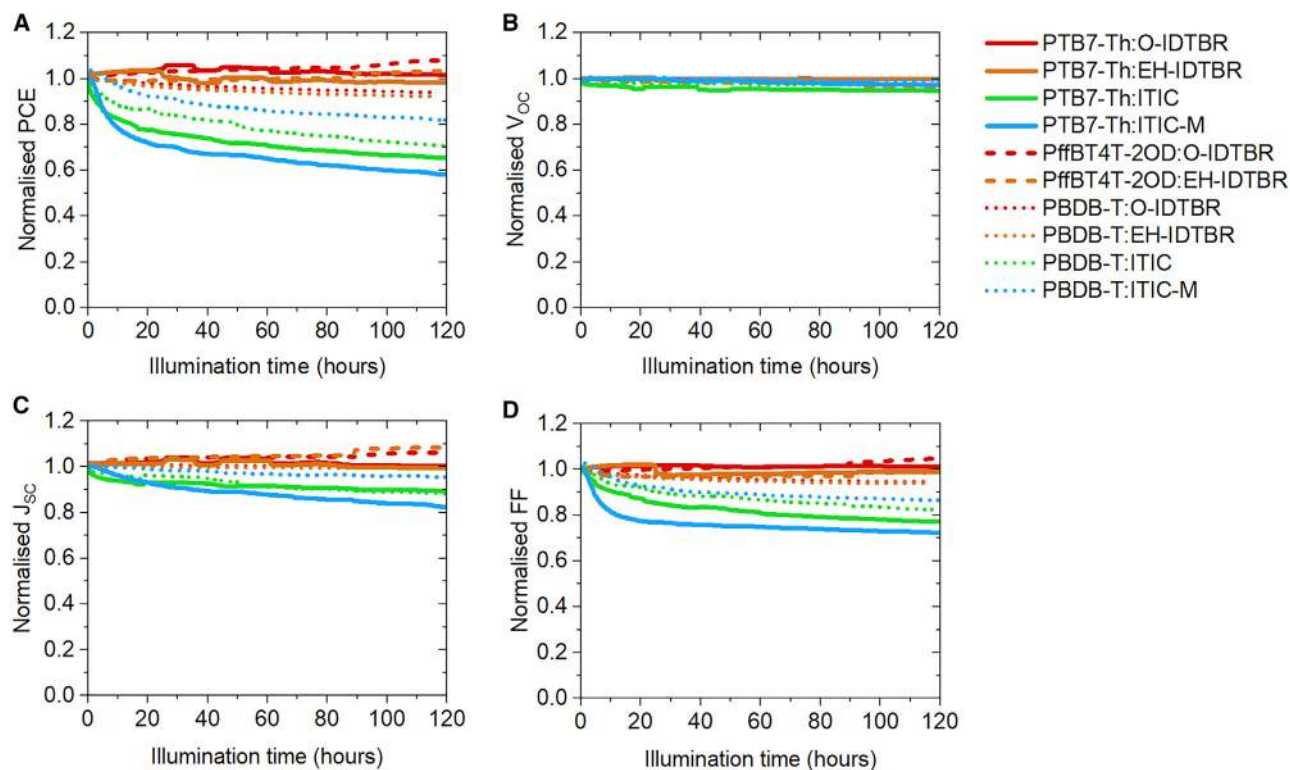
**Figure 2. Photostability of investigated devices**
(A–D) Normalized PCE (A), $V_{OC}$ (B), $J_{SC}$ (C), and FF (D) of investigated devices during continuous photoexcitation under 1 sun equivalent intensity white LED irradiation. Devices were kept in a nitrogen atmosphere for the duration of the test.

degradation for all investigated OSC systems.[52] The effective drift mobility of these NFAs was measured by charge extraction methods under short-circuit conditions,[54] as shown in Figure 3B. The reduction in effective mobility of PTB7-Th:ITIC and PTB7-Th:ITIC-M OSCs upon degradation suggests an increase in hopping steps during transport. The magnitude of the decrease in effective mobility is in good agreement with the increase in charge carrier lifetime measured at open circuit (shown in Figure S2). This suggests that the additional tail states are acting as traps that must first undergo thermally activated detrapping before recombining, thereby leading to the observed increase in lifetime and decrease in mobility. In contrast, no noticeable change in effective mobility is seen for PTB7-Th:O-IDTBR and PTB7-Th:EH-IDTBR OSCs, consistent with their excellent photostability.

## Optical studies

To investigate photo-induced changes to the optical properties of the investigated materials, UV-visible spectra of blend and neat films were measured. To probe the intrinsic photostability of the donor and acceptor components, we focused on the investigation of neat films, as shown in Figure 4. All prolonged photoexcitation was carried out under 1 sun equivalent intensity white LED illumination inside a nitrogen-filled glovebox with oxygen and moisture levels below 0.5 ppm. UV-visible spectra of fresh films were measured and subsequently repeated after 1 and 7 days of continuous photoexcitation, corresponding to the burn-in period and beyond.

After 7 days of continuous photoexcitation, no observable change was seen in the absorbance of PTB7-Th (Figure 4A), indicating that the donor polymer was not
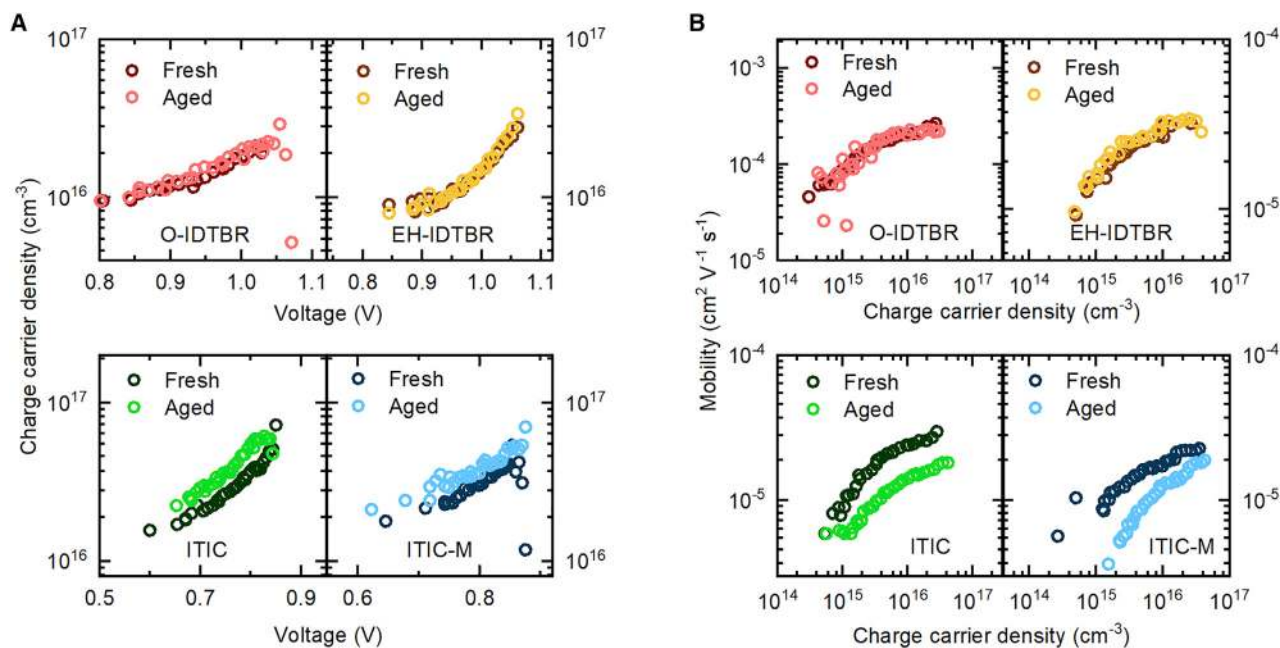
**Figure 3. Energetics and effective charge carrier mobilities of PTB7-Th:NFA devices**
(A) Measurements of the accumulated charge density at open-circuit voltage as a function of illumination intensities, determined by charge extraction.
(B) Effective drift mobility as a function of charge carrier density determined by charge extraction measured at the short-circuit current.
Devices labeled "aged" were exposed to 24 h of continuous illumination under the same conditions as the stability measurements.

significantly contributing to the burn-in and subsequent degradation of the OSCs. Both O-IDTBR and EH-IDTBR exhibited excellent photochemical stability with negligible degradation upon photoaging (Figures 4B and 4C), consistent with the outstanding stability of O-IDTBR and EH-IDTBR OSCs. In contrast, a noticeable loss of absorption was observed for both ITIC and ITIC-M after just one day of continuous photoexcitation (Figures 4D and 4E). This continued with increased photoaging time. A slight increase in the absorbance between 430 and 550 nm was also observed (Figure S3). These observations indicate bleaching of the chromophores and disruption/shortening of the conjugation length of ITIC and ITIC-M upon continuous photoexcitation. Such changes in optical properties are in agreement with the observed losses of $J_{SC}$ and efficiency of ITIC and ITIC-M-based OSCs during the burn-in period and beyond. This bleaching is similar to the bleaching caused by photo-induced dimerization of fullerenes, which also results in a rapid loss in $J_{SC}$ of fullerene-based OSCs,[29] and photobleaching of IDFBR, which was found to originate from fragmentation during continuous illumination in both air and nitrogen.[26] Figure 4 focuses on neat donor and acceptor films, but similar behavior is observed in blend films, although the rate of photodegradation is reduced (Figure S4). The slower degradation in the blend is a result of the overlapping absorption of the donor and acceptor, which means that the acceptor absorbs relatively less light compared with the neat films. In addition, if the degradation mechanism goes via the excited state, as reported previously for other OSC materials,[26,55,56] it would be suppressed in the blend due to charge-transfer (CT) quenching the excited state.

### Structural investigations

To identify the molecular origins of such optical property changes, resonant molecular vibrational Raman spectroscopy was used. Raman spectroscopy has been previously used to study the degradation of organic photovoltaic materials, providing key information about photo-induced chemical and conformational changes and
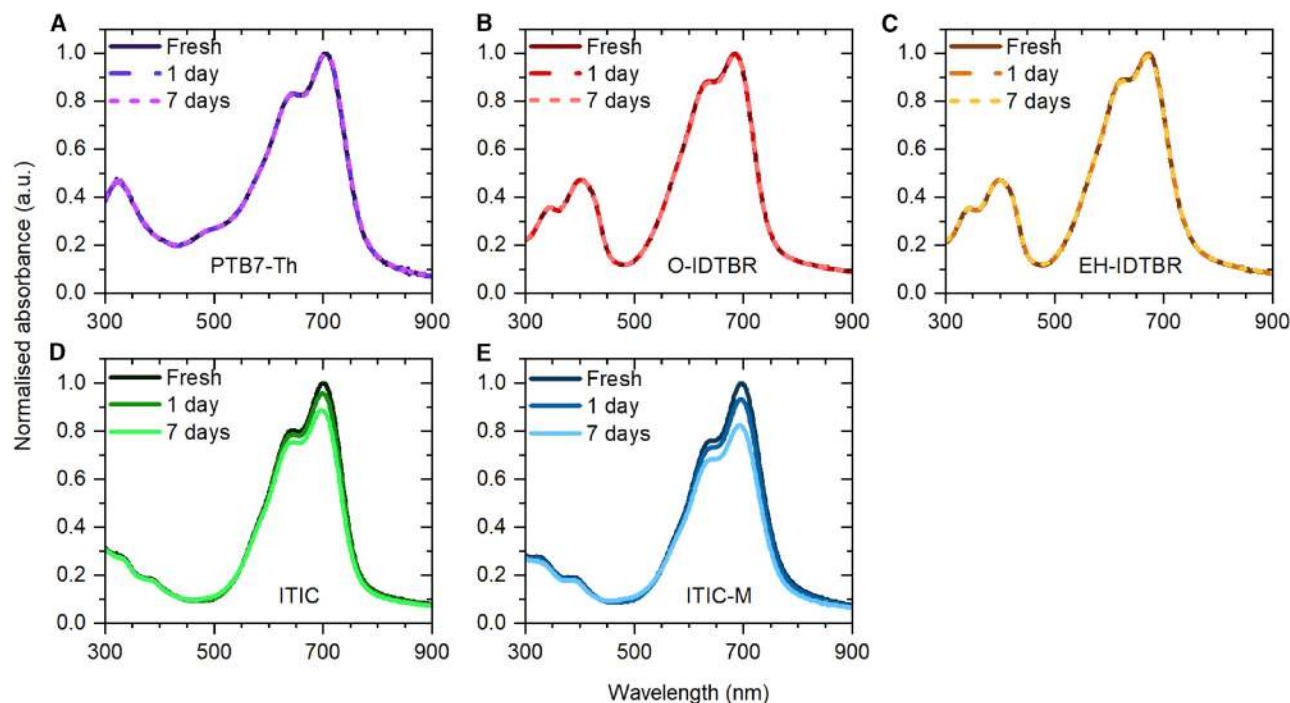
**Figure 4. UV-visible spectra of donor and acceptor films before and after extended photoexcitation**
PTB7-Th (A), O-IDTBR (B), EH-IDTBR (C), ITIC (D), and ITIC-M (E). Continuous photoexcitation was performed inside a nitrogen-filled glovebox, with a 1 sun equivalent intensity white LED array as the illumination source. All spectra are normalized to the fresh spectrum of the corresponding material. For PTB7-Th, O-IDTBR, and EH-IDTBR, all spectra are overlapping, because there is no change in absorbance during continuous photoexcitation.

their origins.[26,57] As shown in Figures 5A–5C, there was no significant change in the Raman spectra of PTB7-Th, O-IDTBR, or EH-IDTBR upon 7 days of photoaging. This corroborates our previous findings of the good photochemical stability of these acceptors when degraded *in situ* under nitrogen.[26] In contrast, both ITIC and ITIC-M exhibit significant changes in their Raman spectra upon photoaging (Figures 5D and 5E). This is indicative of more severe photochemical degradation of ITIC and ITIC-M compared with O-IDTBR and EH-IDTBR and is in agreement with the UV-visible spectral changes and device stability measurements. Although some subtle changes are observed after 1 day of photoaging for ITIC and ITIC-M (Figures S5 and S6), these changes become more evident with increasing photoaging time, indicating that the associated degradation processes continue beyond the burn-in period. Raman spectra of ITIC and ITIC-M up to 2,250 cm$^{-1}$ are shown in Figures S7 and S8.

Overall, there is an increase in Raman intensity for both ITIC and ITIC-M when probed at both 457 and 514 nm. This indicates the formation of a new, wider-band-gap, Raman active-degradation product that is resonant at these wavelengths, in agreement with the slight increase in the absorption of degraded molecules at these wavelengths (Figure S3). To identify the changes in specific molecular vibrations upon prolonged photoexcitation and understand the nature of this degradation product, the difference spectra between the fresh and the degraded films were extracted and are shown in Figures 5F and 5G. These difference spectra highlight the peaks associated with the degradation products whose intensities increase because of the resonant effect of the degradation product under 457 and 514 nm excitation. Both ITIC and ITIC-M show the same changes in molecular vibrations, signifying the same degradation process is occurring in both molecules. The nature
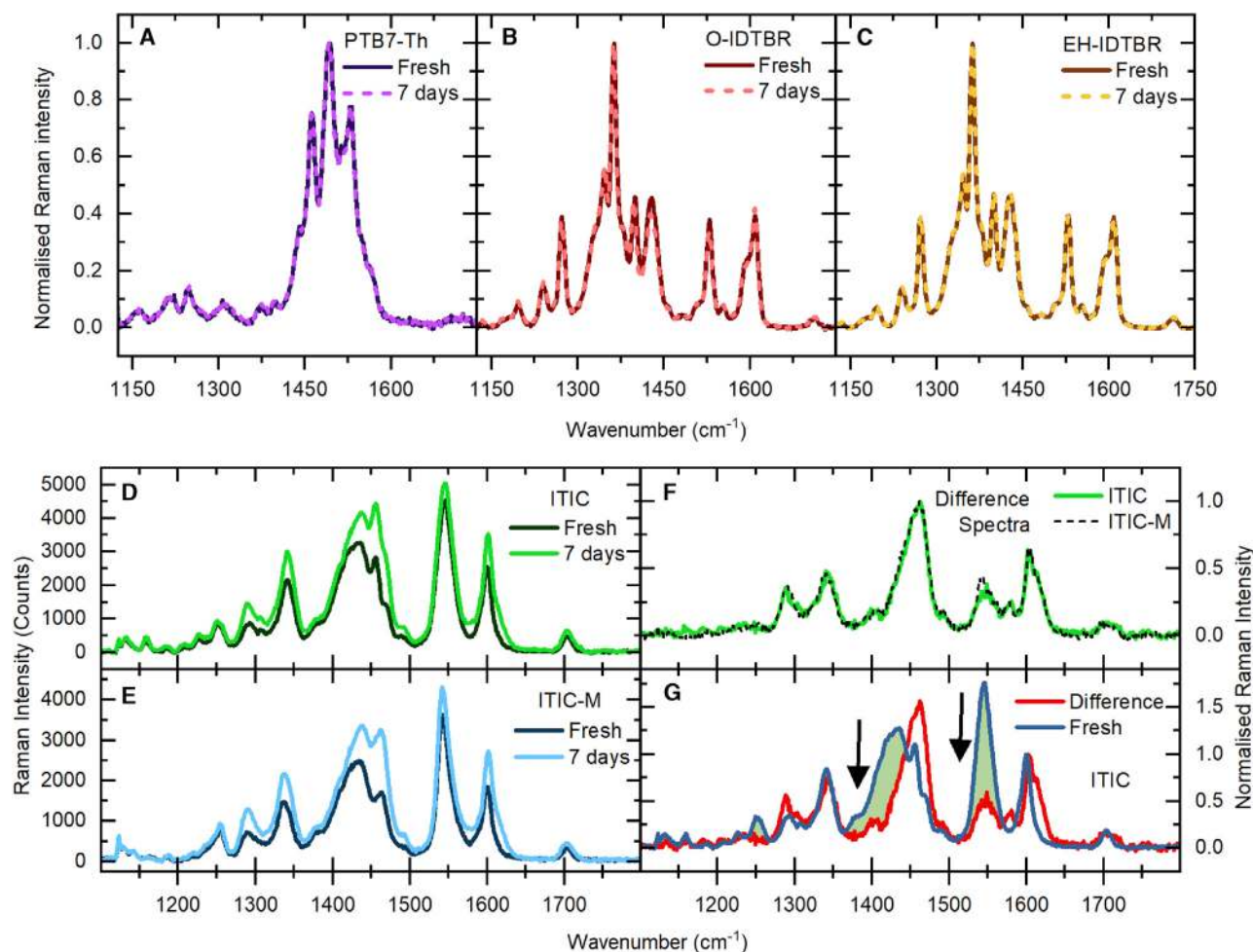
**Figure 5. Raman spectra of neat donor and acceptor films before and after extended photoexcitation**

(A–C) Normalized Raman spectra of PTB7-Th (A), O-IDTBR (B), and EH-IDTBR (C) films before and after 7 days of continuous photoexcitation.

(D and E) Raman spectra of ITIC (D) and ITIC-M (E) films before and after 7 days of continuous photoexcitation. An additional peak at 2,220 cm$^{-1}$ is shown in Figures S7 and S8.

(F) Normalized difference spectra of the fresh and 7 day aged films for both ITIC and ITIC-M.

(G) Normalized difference and fresh spectra of ITIC.

All spectra were measured under a nitrogen atmosphere with a 514 nm excitation laser.

of these peaks was identified using density functional theory (DFT) calculations (Figures S9 and S10). There are some important differences between fresh and degraded ITIC: the alkene peak at 1,550 cm$^{-1}$ and the thiophene peak at 1,425 cm$^{-1}$ are significantly quenched in the degradation product, along with the nitrile peak at 2,220 cm$^{-1}$ (shown in Figure S7). In addition, a new peak at 1,580 cm$^{-1}$, possibly a new alkene mode, is seen to grow in. The peak at 1,455 cm$^{-1}$ appears to gain intensity and shift to higher frequencies; this shift to higher frequency is seen for other peaks, including the core phenyl peak at 1,600 cm$^{-1}$. These peak changes are also seen when probed at 457 nm (Figure S11).

These Raman peak changes indicate important chemical and structural changes of the NFAs upon prolonged photoexcitation. To demonstrate these peak changes more clearly, we conducted *in situ* accelerated photodegradation of ITIC in a nitrogen-filled chamber. *In situ* degradation allows us to track peak changes continuously and hence determine the exact nature of molecular structure changes upon
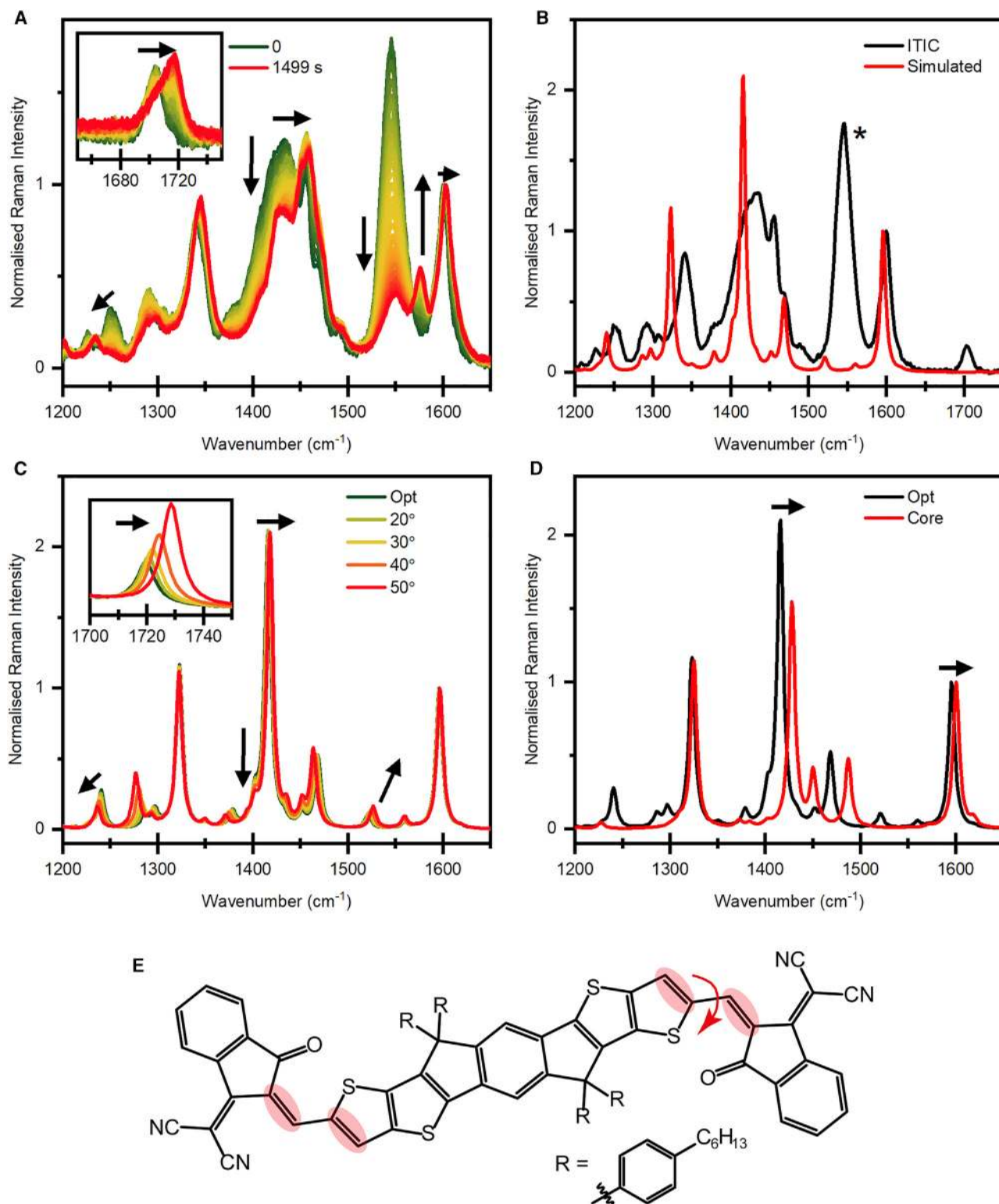
**Figure 6. *In situ* Raman spectra of ITIC during laser degradation and simulated Raman spectra**

(A) Baselined and normalized *in situ* Raman spectra taken at increasing laser degradation times under a nitrogen flow at 514 nm excitation. Arrows show the main peak changes upon degradation.

(B) Simulated Raman spectra of ITIC in its optimized lowest-energy geometry (Opt) versus experimental fresh ITIC Raman spectra. The main alkene peak is marked with an asterisk.

photoexcitation.[20,26] It also provides photodegradation accelerated by high-intensity laser irradiation, which allows us to ensure reproducibility on a shorter timescale and provides a more extreme situation of degradation, which assists with interpretation. The baselined and normalized Raman spectra at increasing degradation times are shown in Figure 6A. There is an increase in Raman intensity and photoluminescence (PL) background across the spectrum (Figure S12), similar to the preceding 7 day photoaged spectra. All changes observed after 7 days of photoaging are observed after *in situ* laser degradation, with some additional changes becoming more apparent: the thiophene C=C peak at 1,250 cm$^{-1}$ is quenched and shifts to lower frequencies, and the carbonyl peak at 1,705 cm$^{-1}$ shows a new high-frequency shoulder growing in. If we take the difference spectra at early degradation times, we obtain a spectrum similar to that shown in Figure 5F, indicating the same degradation process is occurring both in prolonged photoaging under white LED illumination and during laser degradation (Figure S12C).

To understand the origin of these changes and their implication to photostability of ITIC, we compare our experimental data to simulated Raman spectra. First, there is an overall good match between the experimental and the simulated spectra. Four regions of vibrations show higher relative intensities in the measured spectra compared with the simulated spectra, but all are present in both (Figure 6B). These regions are the alkene peak at 1,550 cm$^{-1}$, which we ascribe to the vinylene linkage; the carbonyl peak at 1,705 cm$^{-1}$ (simulated peak highlighted in Figure S10); the thiophene region around 1,450 cm$^{-1}$; and the nitrile peak at 2,220 cm$^{-1}$ (shown in Figure S7). One of these peaks, the alkene at 1,550 cm$^{-1}$, shows a large reduction in relative peak intensity upon degradation. When diluted films of ITIC are fabricated by blending with polystyrene, this peak is reduced in relative peak intensity, demonstrating the alkene's sensitivity to intermolecular packing (Figure S13). Upon degradation, the decrease in relative intensity of this peak indicates disruption of ITIC packing.

To understand the other peak changes upon degradation, we explored several degradation products. One proposed mechanism that correlates well with the changes in the measured Raman spectra, alongside the observed photobleaching, is that of photo-induced conformational change affecting the end groups of the molecules. To verify this conformational instability of ITIC as the main cause for its photoaging, we simulated the Raman changes of ITIC with an increasing dihedral angle between the core and the end groups, rotating about the single bond on the vinylene linkage (Figure 6C, dihedral labeled in Figure 6E). As the molecule is made less planar, the carbonyl and alkene peaks shift to higher frequency, accounting for the new high-frequency peaks observed experimentally. Alongside these new peaks, there is a shift to lower frequencies and quenching of the peak at 1,250 cm$^{-1}$, quenching of the shoulder of the 1,400 cm$^{-1}$ peak, and a slight shift of the peak at 1,450 cm$^{-1}$, as observed experimentally. This agreement between simulated and experimentally measured spectra confirms that the end groups are responsible for photoaging. Such conformational changes of ITIC from a planar to a twisted structure will shorten the effective conjugation length of the molecule. The decrease in absorption at low energy and the slight increase in absorption at higher energies might reflect such changes (Figures 4 and S3).

(C) Simulated Raman spectra at increasing dihedral angles across the single C-C bond in the vinylene linkage. Arrows highlight the main peak changes that are consistent with those observed experimentally.

(D) Simulated Raman spectra of ITIC and the fused indacenodithiophene core, i.e., after loss of the end groups. Arrows highlight the main peak changes that are consistent with those observed experimentally.

(E) Chemical structure of ITIC, highlighting the main vibrational modes that are affected by photoaging. The red arrow indicates the dihedral angle modified in (C).

**CellPress**
OPEN ACCESS

Our previous studies show that conformational change can lead to bond breaking,[26] which can also cause shortening of the effective conjugation length. To probe this, we simulated Raman changes when the vinylene linkage is broken and end groups are lost (the simulated core spectrum shown in Figure 6D). The peaks at 1,420 and 1,600 cm$^{-1}$ show larger shifts to higher frequency than those induced by conformational change, which is again consistent with the experimentally observed changes. In addition, the peaks corresponding to the end groups (i.e., the alkene, carbonyl, and nitrile) are quenched. Therefore, we can draw the clear conclusion that there is a reduction in the effective conjugation length. This loss of conjugation of ITIC and ITIC-M molecules originates from the vinylene linkage between the electron-donating core and the electron-deficient end group, consistent with the reported chemically unstable nature of this linkage.[28,41,42] Importantly, we find that even in an inert atmosphere, this unstable vinylene linkage, which is particularly sensitive to intermolecular packing, is vulnerable to conformational change. Such conformational change will eventually lead to irreversible bond breaking, shortening the effective conjugation breaking of ITIC and ITIC-M. It appears that modification of the substituents on the end group, i.e., by methylation, which affects intermolecular packing or electron-withdrawing strength,[7] influences the stability of this interunit region (depicted in Figure S5). This is in agreement with previous studies that indicated methylation of ITIC leads to poorer stability.[37]

Raman spectra were also measured for blend films (Figure S14). In the case of blend films, no obvious changes were observed after 7 days of photoaging. This is not too surprising, given the slower rate of degradation within the blends compared with neat films, as evidenced by UV-visible spectroscopy (Figures 4 and S4). For neat films, it was shown that *in situ* degradation using the Raman excitation laser as the light source caused the same degradation as observed after prolonged photoexcitation under the white LED source (Figure S12), albeit at a faster rate. When blend films were degraded *in situ* with the Raman excitation laser in a nitrogen environment, the same peak changes were observed in the blend as were observed for the neat films, demonstrating that the same degradation process is occurring in the blend, despite the slower rate of degradation (Figure S15).

### Luminescence studies

PL and electroluminescence (EL) measurements were also performed on the PTB7-Th:NFA devices before and after 24 h of continuous photoexcitation, covering the burn-in period (Figure 7). PL and EL emission from OSCs can be affected by numerous factors. For example, PL is sensitive to changes that affect the absorption properties of the photoactive materials, exciton diffusion behavior, and exciton dissociation, whereas EL can be affected by changes in the energetics of various layers, carrier mobility, and trapping behavior. All of these properties are in turn sensitive to the photoactive-layer morphology, meaning it is not always straightforward to determine the responsible factor that leads to changes in PL and EL spectra; nevertheless, the techniques can provide complimentary evidence alongside other experimental techniques and may help to suggest potential degradation pathways.

For both PTB7-Th:O-IDTBR and PTB7-Th:EH-IDTBR OSCs, no significant change (less than 10% increase in intensity) in PL emission was observed after 24 h of continuous photoexcitation. Combined with the negligible changes in EL emission of these devices, this provides further evidence that the constituent materials are stable. Due to the sensitive nature of these techniques to small changes in morphology and transport behavior, these data also suggests that there are no obvious changes to
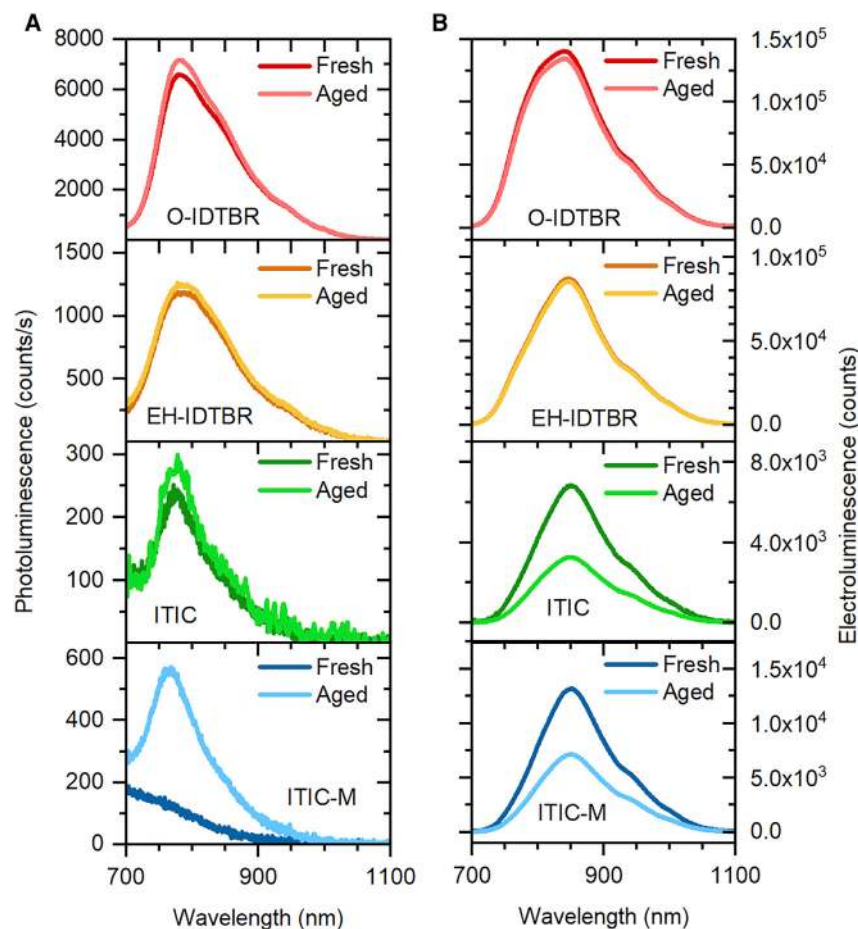
**Figure 7. Photoluminescence and electroluminescence spectra of PTB7-Th:NFA devices before and after extended photoexcitation**

(A and B) Photoluminescence (A) and electroluminescence (B) spectra of PTB7-Th:NFA devices before and after 24 h of continuous photoexcitation under the same conditions as were used during stability measurements. The slight difference in the shape of the fresh PTB7-Th:ITIC-M device PL peak results from its low emission, which is slightly distorted by the small amount of emission from the encapsulation glue (glue emission shown in Figure S16).

the morphology of the photoactive layer during the initial burn-in period. This is consistent with the observed burn-in-free, excellent device stability of these blends and agrees well with previous reports by others of the good morphological stability of the PTB7-Th:EH-IDTBR blend.[34]

For the PTB7-Th:ITIC device, although there may be a slight increase in PL emission, changes of this kind are relatively small. A larger 3.5-fold increase was observed for the PTB7-Th:ITIC-M device after this period of continuous photoexcitation. The slight difference in the shape of the fresh PTB7-Th:ITIC-M device PL peak results from its low emission, which is slightly distorted by the small amount of emission from the encapsulation glue (glue emission shown in Figure S16). Comparison of the blend emission with neat material PL (Figure S17) indicated that the observed blend PL emission originates from donor and/or acceptor excitons, rather than from CT-state emission. This means that after a period of prolonged photoexcitation, there is an increase in the number of photogenerated excitons that proceed to radiatively recombine within the PTB7-Th:ITIC-M device.

## Cell Reports
# Physical Science
### Article

Several factors may cause such an increase in PL emission. For example, the observed changes in intermolecular interactions and conformational changes of ITIC and ITIC-M outlined previously may inhibit exciton diffusion and/or dissociation, leading to an increase in the number of excitons that radiatively recombine. Changes to the morphology of the blend during continuous photoexcitation may also contribute to the observed increases in PL emission.[58–61] Morphological changes have been widely reported to be responsible for burn-in degradation for several OSC blends, including demixing of amorphous regions for both polymer:fullerene[32,33,62] and polymer:NFA[34,63,64] devices, as well as crystallization and diffusion-limited aggregation of NFAs.[42,43,62,63] Recently, transmission electron microscopy (TEM) imaging of PTB7-Th:ITIC films before and after photoaging under similar conditions to those used in this work suggested that demixing likely occurs in this blend linked with poor miscibility between donor and acceptor.[34] Increases in PL emission, as observed here, were also reported and may be explained by the coarsening of domains, leading to a reduced probability of exciton dissociation.[34] To probe the possibility of large-scale phase segregation, atomic force microscopy (AFM) measurements were carried out on PTB7-Th:ITIC and PTB7-Th:ITIC-M films before and after 7 days of continuous photoexcitation with a 1 sun equivalent intensity white LED source in a nitrogen environment (Figure S18). No clear changes in the AFM images were observed after 7 days of photoaging. This suggests that there is no obvious large-scale phase separation.

The conformational changes of ITIC and ITIC-M may explain the increase in PL emission upon photodegradation of the blend. Although exciton emission from the neat ITIC and ITIC-M decreases upon photodegradation (Figure S19), the resulting disruption to packing and energetics, as a result of conformational changes, can cause an increase in PL of the blend by hindering exciton dissociation, resulting in more excitonic emission. We also cannot rule out more subtle morphological changes. For example, ITIC has also been observed to reorientate from more face-on to more edge-on orientation during photoexcitation under nitrogen.[37] Additionally, diffusion-limited NFA aggregation, leading to the formation of isolated acceptor domains, has also been reported for ITIC-4F.[43] Such changes in morphology could also contribute to an increase in PL emission and may act alongside the photo-induced chemical degradation reported herein.

Contrasting the PTB7-Th:O-IDTBR and PTB7-Th:EH-IDTBR devices, a ~50% reduction in EL emission is observed for PTB7-Th:ITIC and PTB7-Th:ITIC-M devices. Given the negligible change in series resistance after extended photoexcitation (Figure S20), the injection of current will cause a similar voltage drop for both fresh and photoaged devices. Therefore, the reduction in emission implies the recombination in the photoactive layer is less radiative. This behavior is consistent with our previously discussed results. This decrease in EL emission can be explained by the observed conformational changes to ITIC and ITIC-M. These changes result in disruption to intermolecular packing, intra- and intermolecular charge transport, and increased energetic disorder and trap formation, thereby causing a reduction in EL emission and correlating well with device stability. The EL emission of the neat materials is shown in Figure S21 for reference.

## DISCUSSION

Photostability is a widely recognized challenge for OSCs, and a detailed understanding of the degradation mechanisms is required to enable the design of high-performance stable OSCs. Our study addresses the photostability of NFA-based OSCs

**CellPress**
OPEN ACCESS

**Cell Reports**
**Physical Science**
Article

and investigates the generality of behavior across a range of donor polymers and electron acceptors. We demonstrate that rational design and choice of suitable electron acceptors, instead of donor polymers, might be a more effective strategy to achieve long-term photostability of OSCs. Through a range of characterization techniques, we show that photochemical stability of NFAs must be addressed for good device stability to be achieved. Due to combined excellent photochemical and likely morphological stability,[34] IDTBR-based OSCs can achieve good photostability with minimal burn-in losses.[30,36] Unfortunately the maximum efficiencies achieved by IDTBR-based acceptors are slightly lower compared with ITIC-based materials. However, despite good device performance, both ITIC and ITIC-M suffer from more severe photochemical degradation of their molecular structure during continuous photoexcitation in inert atmospheres, leading to poor device stability.

We find that ITIC and ITIC-M degrade in the same way during continuous photoexcitation. We observe several key changes in the Raman spectra that, alongside simulated Raman spectra, allow us to explain the location of this photodegradation, namely, the interunit region, and propose the mechanism behind it. An initial conformational change—specifically, twisting of the end group (the single bond that connects the core to the end groups)—is observed, which can lead to the more extreme situation in which the vinylene linkage breaks. Gas-phase single-molecule DFT simulations of these proposed alterations show similar outcomes in both situations and agree with the changes observed experimentally. Such changes would reduce the effective conjugation length of the molecule, in agreement with the decrease in the main UV-visible absorption peaks of ITIC and ITIC-M upon photoaging (Figures 4D and 4E), alongside a slight increase in higher-energy absorption (Figure S3). These changes would also affect molecular packing, which is observed by the decrease in the relative intensity of the Raman peaks sensitive to intermolecular packing. The methylation of the end group, which affects intermolecular packing or electron-withdrawing strength,[7] may also affect the stability of this interunit region, with ITIC-M appearing to suffer from more rapid degradation compared with ITIC, as shown by the larger changes in both UV-visible (Figure 4) and PL (Figure S19) spectra of neat materials after a period of continuous photoaging. These changes are reflected in the overall Raman intensity increase (Figures 5D, 5E, and S5) associated with the slight increase in absorption at the probing wavelengths (Figure S3), which is indicative of the formation of a degradation product with a wider band gap. In agreement with previous reports,[37] this suggests that the strategy of methylation to improve the performance of ITIC may compromise the photostability of ITIC-based OSCs, although intermolecular interactions and different morphologies in the blend may also affect the rate of photodegradation in devices.

We consider the potential impact of the different 3D packing structures observed for IDTBR and ITIC acceptors on the photo-induced conformational changes. Despite π-stacking distances being similar in their crystal structures,[65,66] the difference in side chains and the resulting stabilizing interactions between them can influence morphological and conformational stability. The flexible aliphatic side chains of IDTBR can pack tightly,[66] maximizing and stabilizing dispersive interactions, whereas the bulky phenyl-hexyl side chains in ITIC are not as conducive to such stable packing. In fact, ITIC has been shown to pack differently in its crystal structure compared with spin-coated thin films, which tend to be more disordered because of these bulky side chains.[67,68] These side chains were designed specifically to reduce molecular planarity and inhibit self-aggregation, which can be detrimental to performance.[5] However, this disorder and comparatively poorer dispersive interactions of the hexyl-phenyl side chains could make ITIC more susceptible to

morphological and conformational changes, leading to poor device stability. Elsewhere, it has been observed that the inclusion of thiophene in the side chains (ITIC-Th) improves crystallinity and packing,[47] which in turn correlates with the observed improved stability of ITIC-Th devices, highlighting the important role that side chain engineering can have with regards to NFA stability.[37]

Within PTB7-Th:ITIC and PTB7-Th:ITIC-M devices, we also observe a distinctly larger increase in PL emission upon photoaging compared with PTB7-Th:O-IDTBR and PTB7-Th:EH-IDTBR devices, and the increase was especially large for ITIC-M. This PL emission originates from donor and/or acceptor excitons, rather than CT-state emission. Such behavior is explained by reduced rates of exciton dissociation. The conformational change of ITIC and ITIC-M will affect both intra- and intermolecular interactions in blends, in turn affecting associated photophysical processes such as charge generation and transport. The disrupted interactions would hinder exciton dissociation in blends, leading to more excitonic emission of the neat materials, as observed in our work. This result highlights the important interplay between molecular conformational stability and molecular-scale morphological stability, in which initial conformational change can disrupt molecular interactions.

Although no macro-scale morphological changes were observed after photodegradation, we cannot exclude the possibility of other morphological instabilities contributing to these observed PL changes, especially with previous reports highlighting the tendency of crystallization and small-scale aggregation of ITIC-based acceptors during aging[43,47] and that the poor miscibility between PTB7-Th and ITIC can lead to demixing of intermixed domains.[34] Such changes may occur in parallel with the photo-induced chemical degradation reported herein, but these changes are not large enough to be probed by AFM measurements. Therefore, our results identify the molecular-scale conformational and morphological changes as critical origins of the photostability of NFAs and NFA-based OSCs. These observations are consistent with the differing stabilities of the investigated devices. Specifically, O-IDTBR and EH-IDTBR are more resistant to photochemical degradation upon continuous photoexcitation in inert atmospheres. Within PTB7-Th devices, the minimal changes in device performance, PL or EL emission, and TPV/CE additionally suggests that the blend morphologies are relatively stable, likely partly because of the stabilizing interactions between the side chains of these acceptors. Consequentially, no obvious changes in charge transport and trapping behavior are observed for these devices, and initial good performance is maintained during continuous illumination.

However, ITIC and ITIC-M appear to suffer photochemical degradation upon continuous illumination in inert atmospheres, associated with twisting about the single bond on the vinylene linkage and possible complete breaking of this link between the core and the end group. These changes reduce the effective conjugation length of the molecules, reducing their absorption and likely affecting packing and intra- and intermolecular charge transport. This, in combination with morphological changes that may occur, can explain the poor device stability and increased charge trapping.

When investigating the differences between ITIC and IDTBR, we noted from quantum chemical simulations (Figure S22) that the charge distribution within ITIC shows a strong intramolecular charge-transfer (ICT) character with a strong dipole moment between the electron-rich core and the electron-withdrawing end groups; however, IDTBR shows a weaker charge distribution. Although this strong ICT character may

**CellPress**
OPEN ACCESS

**Cell Reports
Physical Science**
Article

improve charge generation,[69] its impact on photochemical stability is unclear and requires further investigation.

Our study highlights the importance of rational NFA molecular design to improve OSC stability. It is necessary for these design rules to complement those for efficiency optimization in the early stages of material design. We have shown that some of the most popular NFAs lack good stability due to their susceptibility to photochemical degradation during illumination, even in inert conditions. In addition, because of the strong dependence of degradation behavior on the choice of NFA and relative independence of donor polymer within our investigated systems, we consider new molecular design of NFAs as a key strategy to improve the stability of OSCs. We propose the following design rules for improved NFA stability. Primarily, we draw attention to the vinylene linkage between the donor core and the acceptor units within ITIC, which we identified as the main point of degradation. Interestingly, the vinylene linkage between electron-withdrawing benzothiadiazole (BT) and rhodanine groups of IDTBR appears to be less prone to degradation. Therefore, the real weak point may be better described as the interunit region between the donor core and the acceptor components about which rotation can occur. This links with our previous studies on IDTBR, where we show that the core-BT linkage is susceptible to degradation,[26] although it is necessary to explore the generality of this further. To stabilize this interunit region, strong conformational lockers could be applied to resist the photoinduced conformational changes that lead to degradation, such as in the chemically similar Y6 NFA, although the impact on device performance in Y6 has yet to be established.[53] In addition, we suggest that to enable stable and resilient packing, bulky side chains should be avoided in favor of alkyl side chains or alternatives with heteroatoms that improve intermolecular interactions. However, we acknowledge that a careful balance may be required to prevent excessive self-aggregation, which can be problematic for highly planar molecules.[5] End-group substitution is another important consideration, and we show that end-group methylation may need to be avoided, although more work is needed to understand the role of end-group methylation on stability. Others have suggested that end-group fluorination, rather than methylation, could be an effective strategy to improve stability.[37] Finally, although molecular design of NFAs is important, the design of matching polymer donors should also be considered with great care, in terms of both their intrinsic stability and their molecular interactions with acceptors, which can determine their miscibility and the morphological stability of devices.[32–34,62–64]

## EXPERIMENTAL PROCEDURES

### Resource availability

#### Lead contact

Further information and requests for resources should be directed to and will be fulfilled by the lead contact, Zhe Li (zhe.li@qmul.ac.uk).

#### Materials availability

No new materials were generated within this work. The full chemical names of the donor and acceptor materials used in this work are provided in Note S1. All donor polymers were purchased from 1-Material. ITIC and ITIC-M were also purchased from 1-Material. O-IDTBR and EH-IDTBR were provided by Prof. I. McCulloch's group. Polystyrene ($M_W$ of 280 kDa), chlorobenzene, chloroform, zinc acetate dihydrate, 2-methoxyethanol, and ethanolamine were purchased from Sigma Aldrich. $MoO_3$ (99.999%) was purchased from Strem Chemicals. Ag (99.999%) was purchased from Kurt J. Lesker. The UV-curable epoxy for encapsulation was supplied by Solarmer Materials. All materials were used as received.

*Data and code availability*
- All data reported in this paper will be shared by the lead contact upon request.
- This paper does not report original code.
- Any additional information required to reanalyze the data reported in this paper is available from the lead contact upon request.

### Device fabrication

Devices were fabricated with the inverted architecture (indium tin oxide [ITO]/ZnO/active layer/$MoO_3$/Ag). Pre-coated and patterned ITO-coated glass substrates were cleaned by ultrasonication in Hellmanex III (2% by volume in deionized water), deionized water, acetone, and isopropanol. After cleaning, substrates were dried with an air gun. Dried substrates were treated with an oxygen plasma. 219.5 mg of zinc acetate dihydrate was dissolved in 2 mL of 2-methoxyethanol and 60.4 μL of ethanolamine overnight at room temperature and was then spin-coated in air at 4,000 rpm onto the substrates and annealed at 150°C for 10 min to form a ~20 nm ZnO layer. The active layer was then deposited by spin coating in a nitrogen-filled glovebox with oxygen and moisture levels below 0.1 ppm. The details of active-layer preparation and deposition can be found in the Table S1. Subsequently, a 10 nm layer of $MoO_3$ and 100 nm layer of silver were deposited via thermal evaporation through a shadow mask as the hole-transporting layer and top electrode, respectively. Devices were encapsulated inside a nitrogen atmosphere with a UV-curable epoxy and a glass cover slide.

### Stability testing

Encapsulated devices were placed into an environmental chamber with a glass front for performance monitoring under continuous illumination. The chamber was purged with nitrogen for at least 30 min before illumination, and positive pressure of nitrogen was maintained by passing an uninterrupted flow of nitrogen through the chamber for the duration of the measurements. A white LED array was used as the light source, with the intensity of the LED array and device position adjusted such that the $J_{SC}$, and hence charge density within each device, was approximately equal to that measured under 1 sun AM1.5G illumination. The spectrum of the LED array is shown in Figure S1. The environment temperature was kept below 30°C by a water-cooling system. During stability measurements, current-voltage responses were measured at least once per hour, and devices were kept under open-circuit conditions between these measurements. The stability test for the PffBT4T-2OD devices was paused around the 92-h mark to reconnect one of the devices that had a poor electrical connection. The devices were kept in the dark during and after reconnection until the chamber had been repurged with nitrogen, after which the LED array was switched back on and the measurements were resumed. The light intensity may have differed by a small amount after reconnection because of slight repositioning of the devices.

### Transient photovoltage and charge extraction

Charge extraction measurements were used to determine the average charge carrier densities in devices under different illumination levels and different biases (open circuit and short circuit in this study). For each device, the desired light intensity, and consequently the initial bias, was provided by a ring of 12 white LEDs capable of up to 5 sun equivalent illumination. After illumination at the desired intensity, the LEDs were switched off and the device was switched to short circuit. The transient voltage was then acquired with a DAQ card connected to a Tektronix TDS3032B oscilloscope. The voltage transients were converted into current transients through Ohm's law. Then the current transients were integrated to obtain the total charge, Q, which was used to calculate the carrier density, n, in the device. During TPV measurements, the devices were held at open-circuit conditions. The same LED source was

used for illumination, and a small optical excitation was provided by a pulsed 532 nm Continuum Minilite Nd:YAG laser with a pulse length of less than 10 ns. This small excitation produced a small voltage transient decay, which was measured on the oscilloscope. The decay was fitted with a mono-exponential to obtain the small perturbation carrier lifetime, which was used to estimate the total charge carrier lifetime within the device.

### Film studies
An identical white LED array that was used for the stability tests was also used for the continuous illumination of thin films for all film-based characterization. For film studies, all continuous photoexcitation was performed inside a nitrogen-filled glovebox with oxygen and moisture levels below 0.5 ppm. Cooling fans circulated nitrogen over the samples to keep the environmental temperature below 30°C.

### UV-visible spectroscopy
A Perkin Elmer Lambda 750 spectrophotometer with an integrating sphere attachment was used for all UV-visible spectroscopy. A bare glass substrate was used for measurement of the reference spectrum.

### Raman spectroscopy
A Renishaw in Via Raman microscope in a backscattering configuration with a 50× objective was used to collect Raman spectra. All measurements were conducted in a nitrogen-purged Linkam sample chamber. All measurements were taken with a defocused laser spot with a radius of ~10 μm. Raman spectra were collected at various wavelengths using an argon ion laser (457, 488, and 514 nm). Acquisition times and laser powers were optimized to give the best spectra but were kept consistent between samples that are directly compared in the text. Spectrometer calibration was conducted using a silicon reference sample, and background PL was subtracted using a polynomial fit. Accelerated *in situ* degradation was carried out with a laser spot of 10 μm and approximate power density of $3.2 \times 10^6$ W m$^{-2}$, giving an acceleration factor of ~3,000× compared with AM1.5G solar illumination.

### Density functional theory calculations
Density functional theory simulations were carried out using Gaussian 09 software on the Imperial College High-Performance Computing Service.[70] Single molecules were modeled in the gas phase at the B3LYP level of theory with the basis set 6-31G(d,p).[71–74] For frequency calculations, alkyl side chains were simplified to methyl groups to reduce computational time. Structures were optimized to a local minimum energy conformation, with frozen dihedral angles used to simulate molecular conformational changes. Calculated frequencies were corrected using an empirical factor of 0.97 for the frequency of vibration.[75] Electrostatic potential distribution was calculated using the Merz-Kollman model with full side chains.[76]

### Photoluminescence and electroluminescence spectroscopy
For luminescence spectroscopy, a custom-built setup was used. For photoluminescence measurements, a 405 nm laser was used as the excitation source. However, for electroluminescence measurements, a Keithley 2400 was used to apply the voltage to the devices and monitor the current. A current density of 200 mA cm$^{-2}$ was applied to the cells, which is sufficiently low to prevent device damage. For both electroluminescence and photoluminescence, an AvaSpec-ULS2048x64 spectrometer was used to detect the emission. A 550 nm long-pass cutoff filter was placed between the sample and the spectrometer to remove the excitation light for photoluminescence measurements.

## Cell Reports
## Physical Science
## Article

**CellPress**
OPEN ACCESS

## AUTHOR CONTRIBUTIONS

Conceptualization, W.C.T., J.-S.K., and Z.L.; methodology, A.J.C., J.L., W.C.T., J.-S.K., and Z.L.; investigation, A.J.C., J.L., R.M., J.W., E.M.S., M.J.N., and A.E.; resources, A.J.C., Y.W., H.K.H.L., H.B., H.C., K.H., F.G., and I.M.; writing – original draft, A.J.C., J.L., R.M., and J.W.; writing – review & editing, A.J.C., J.L., R.M., J.W., E.M.S., H.B., H.H., U.S.S., J.R.D., W.C.T., J.-S.K., and Z.L.; supervision, F.G., H.H., I.M., U.S.S., T.M.W., J.R.D., W.C.T., J.-S.K., and Z.L.

## DECLARATION OF INTERESTS

The authors declare no competing interests.

## REFERENCES

1. Holliday, S., Ashraf, R.S., Nielsen, C.B., Kirkus, M., Röhr, J.A., Tan, C.-H., Collado-Fregoso, E., Knall, A.-C., Durrant, J.R., Nelson, J., and McCulloch, I. (2015). A rhodanine flanked nonfullerene acceptor for solution-processed organic photovoltaics. J. Am. Chem. Soc. 137, 898–904.

2. Holliday, S., Ashraf, R.S., Wadsworth, A., Baran, D., Yousaf, S.A., Nielsen, C.B., Tan, C.-H., Dimitrov, S.D., Shang, Z., Gasparini, N., et al. (2016). High-efficiency and air-stable P3HT-based polymer solar cells with a new non-fullerene acceptor. Nat. Commun. 7, 11585.

3. Wadsworth, A., Moser, M., Marks, A., Little, M.S., Gasparini, N., Brabec, C.J., Baran, D., and McCulloch, I. (2019). Critical review of the molecular design progress in non-fullerene electron acceptors towards commercially viable organic solar cells. Chem. Soc. Rev. 48, 1596–1625.

4. Yao, H., Chen, Y., Qin, Y., Yu, R., Cui, Y., Yang, B., Li, S., Zhang, K., and Hou, J. (2016). Design and Synthesis of a Low Bandgap Small Molecule Acceptor for Efficient Polymer Solar Cells. Adv. Mater. 28, 8283–8287.

5. Lin, Y., Wang, J., Zhang, Z.-G., Bai, H., Li, Y., Zhu, D., and Zhan, X. (2015). An electron acceptor challenging fullerenes for efficient polymer solar cells. Adv. Mater. 27, 1170–1174.

6. Lin, Y., Zhao, F., He, Q., Huo, L., Wu, Y., Parker, T.C., Ma, W., Sun, Y., Wang, C., Zhu, D., et al. (2016). High-Performance Electron Acceptor with Thienyl Side Chains for Organic Photovoltaics. J. Am. Chem. Soc. 138, 4955–4961.

7. Li, S., Ye, L., Zhao, W., Zhang, S., Mukherjee, S., Ade, H., and Hou, J. (2016). Energy-Level Modulation of Small-Molecule Electron Acceptors to Achieve over 12% Efficiency in Polymer Solar Cells. Adv. Mater. 28, 9423–9429.

8. Zhao, W., Li, S., Yao, H., Zhang, S., Zhang, Y., Yang, B., and Hou, J. (2017). Molecular Optimization Enables over 13% Efficiency in

Organic Solar Cells. J. Am. Chem. Soc. *139*, 7148–7151.

9. Yuan, J., Zhang, Y., Zhou, L., Zhang, G., Yip, H.-L., Lau, T.-K., Lu, X., Zhu, C., Peng, H., Johnson, P.A., et al. (2019). Single-Junction Organic Solar Cell with over 15% Efficiency Using Fused-Ring Acceptor with Electron-Deficient Core. Joule *3*, 1140–1151.

10. Liu, Q., Jiang, Y., Jin, K., Qin, J., Xu, J., Li, W., Xiong, J., Liu, J., Xiao, Z., Sun, K., et al. (2020). 18% Efficiency organic solar cells. Sci. Bull. (Beijing) *65*, 272–275.

11. Li, Y., Lin, J.-D., Che, X., Qu, Y., Liu, F., Liao, L.-S., and Forrest, S.R. (2017). High Efficiency Near-Infrared and Semitransparent Non-Fullerene Acceptor Organic Photovoltaic Cells. J. Am. Chem. Soc. *139*, 17114–17119.

12. Lee, H.K.H., Li, Z., Durrant, J.R., and Tsoi, W.C. (2016). Is organic photovoltaics promising for indoor applications? Appl. Phys. Lett. *108*, 253301.

13. Lee, H.K.H., Wu, J., Barbé, J., Jain, S.M., Wood, S., Speller, E.M., Li, Z., Castro, F.A., Durrant, J.R., and Tsoi, W.C. (2018). Organic photovoltaic cells—promising indoor light harvesters for self-sustainable electronics. J. Mater. Chem. A Mater. Energy Sustain. *6*, 5618–5626.

14. Baran, D., Kirchartz, T., Wheeler, S., Dimitrov, S., Abdelsamie, M., Gorman, J., Ashraf, R.S., Holliday, S., Wadsworth, A., Gasparini, N., et al. (2016). Reduced voltage losses yield 10% efficient fullerene free organic solar cells with >1 V open circuit voltages. Energy Environ. Sci. *9*, 3783–3793.

15. Xue, R., Zhang, J., Li, Y., and Li, Y. (2018). Organic Solar Cell Materials toward Commercialization. Small *14*, e1801793.

16. Speller, E.M., Clarke, A.J., Luke, J., Lee, H.K.H., Durrant, J.R., Li, N., Wang, T., Wong, H.C., Kim, J.-S., Tsoi, W.C., et al. (2019). From fullerene acceptors to non-fullerene acceptors: prospects and challenges in the stability of organic solar cells. J. Mater. Chem. A Mater. Energy Sustain. *7*, 23361–23377.

17. Cheng, P., and Zhan, X. (2016). Stability of organic solar cells: challenges and strategies. Chem. Soc. Rev. *45*, 2544–2582.

18. Jørgensen, M., Norrman, K., and Krebs, F.C. (2008). Stability/degradation of polymer solar cells. Sol. Energy Mater. Sol. Cells *92*, 686–714.

19. Rafique, S., Abdullah, S.M., Sulaiman, K., and Iwamoto, M. (2018). Fundamentals of bulk heterojunction organic solar cells: An overview of stability/degradation issues and strategies for improvement. Renew. Sustain. Energy Rev. *84*, 43–53.

20. Razzell-Hollis, J., Wade, J., Tsoi, W.C., Soon, Y., Durrant, J., and Kim, J.-S. (2014). Photochemical stability of high efficiency PTB7:PC 70 BM solar cell blends. J. Mater. Chem. A Mater. Energy Sustain. *2*, 20189–20195.

21. Wood, S., Wade, J., Shahid, M., Collado-Fregoso, E., Bradley, D.D.C., Durrant, J.R., Heeney, M., and Kim, J.-S. (2015). Natures of optical absorption transitions and excitation energy dependent photostability of

diketopyrrolopyrrole (DPP)-based photovoltaic copolymers. Energy Environ. Sci. *8*, 3222–3232.

22. Sai, N., Leung, K., Zádor, J., and Henkelman, G. (2014). First principles study of photo-oxidation degradation mechanisms in P3HT for organic solar cells. Phys. Chem. Chem. Phys. *16*, 8092–8099.

23. Golovnin, I.V., Bakulin, A.A., Zapunidy, S.A., Nechvolodova, E.M., and Paraschuk, D.Y. (2008). Dramatic enhancement of photo-oxidation stability of a conjugated polymer in blends with organic acceptor. Appl. Phys. Lett. *92*, 243311.

24. Lee, H.K.H., Telford, A.M., Röhr, J.A., Wyatt, M.F., Rice, B., Wu, J., de Castro Maciel, A., Tuladhar, S.M., Speller, E., McGettrick, J., et al. (2018). The role of fullerenes in the environmental stability of polymer:fullerene solar cells. Energy Environ. Sci. *11*, 417–428.

25. Speller, E.M., Clarke, A.J., Aristidou, N., Wyatt, M.F., Francàs, L., Fish, G., Cha, H., Lee, H.K.H., Luke, J., Wadsworth, A., et al. (2019). Toward Improved Environmental Stability of Polymer:Fullerene and Polymer:Nonfullerene Organic Solar Cells: A Common Energetic Origin of Light- and Oxygen-Induced Degradation. ACS Energy Lett. *4*, 846–852.

26. Luke, J., Speller, E.M., Wadsworth, A., Wyatt, M.F., Dimitrov, S., Lee, H.K.H., Li, Z., Tsoi, W.C., McCulloch, I., Bagnis, D., et al. (2019). Twist and Degrade—Impact of Molecular Structure on the Photostability of Nonfullerene Acceptors and Their Photovoltaic Blends. Adv. Energy Mater. *9*, 1803755.

27. Speller, E.M., McGettrick, J.D., Rice, B., Telford, A.M., Lee, H.K.H., Tan, C.-H., De Castro, C.S., Davies, M.L., Watson, T.M., Nelson, J., et al. (2017). Impact of Aggregation on the Photochemistry of Fullerene Films: Correlating Stability to Triplet Exciton Kinetics. ACS Appl. Mater. Interfaces *9*, 22739–22747.

28. Guo, J., Wu, Y., Sun, R., Wang, W., Guo, J., Wu, Q., Tang, X., Sun, C., Luo, Z., Chang, K., et al. (2019). Suppressing photo-oxidation of non-fullerene acceptors and their blends in organic solar cells by exploring material design and employing friendly stabilizers. J. Mater. Chem. A Mater. Energy Sustain. *7*, 25088–25101.

29. Heumueller, T., Mateker, W.R., Distler, A., Fritze, U.F., Cheacharoen, R., Nguyen, W.H., Biele, M., Salvador, M., von Delius, M., Egelhaaf, H.-J., et al. (2016). Morphological and electrical control of fullerene dimerization determines organic photovoltaic stability. Energy Environ. Sci. *9*, 247–256.

30. Cha, H., Wu, J., Wadsworth, A., Nagitta, J., Limbu, S., Pont, S., Li, Z., Searle, J., Wyatt, M.F., Baran, D., et al. (2017). An Efficient, "Burn in" Free Organic Solar Cell Employing a Nonfullerene Electron Acceptor. Adv. Mater. *29*, 1701156.

31. Heumueller, T., Burke, T.M., Mateker, W.R., Sachs-Quintana, I.T., Vandewal, K., Brabec, C.J., and McGehee, M.D. (2015). Disorder-Induced Open-Circuit Voltage Losses in Organic Solar Cells During Photoinduced Burn-In. Adv. Energy Mater. *5*, 1500111.

32. Li, N., Perea, J.D., Kassar, T., Richter, M., Heumueller, T., Matt, G.J., Hou, Y., Güldal, N.S., Chen, H., Chen, S., et al. (2017). Abnormal

strong burn-in degradation of highly efficient polymer solar cells caused by spinodal donor-acceptor demixing. Nat. Commun. *8*, 14541.

33. Zhang, C., Heumueller, T., Leon, S., Gruber, W., Burlafinger, K., Tang, X., Perea, J.D., Wabra, I., Hirsch, A., Unruh, T., et al. (2019). A top-down strategy identifying molecular phase stabilizers to overcome microstructure instabilities in organic solar cells. Energy Environ. Sci. *12*, 1078–1087.

34. Xiao, J., Ren, M., Zhang, G., Wang, J., Zhang, D., Liu, L., Li, N., Brabec, C.J., Yip, H.-L., and Cao, Y. (2019). An Operando Study on the Photostability of Nonfullerene Organic Solar Cells. Sol. RRL *3*, 1900077.

35. Schaffer, C.J., Palumbiny, C.M., Niedermeier, M.A., Jendrzejewski, C., Santoro, G., Roth, S.V., and Müller-Buschbaum, P. (2013). A direct evidence of morphological degradation on a nanometer scale in polymer solar cells. Adv. Mater. *25*, 6760–6764.

36. Gasparini, N., Salvador, M., Strohm, S., Heumueller, T., Levchuk, I., Wadsworth, A., Bannock, J.H., de Mello, J.C., Egelhaaf, H.-J., Baran, D., et al. (2017). Burn-in Free Nonfullerene-Based Organic Solar Cells. Adv. Energy Mater. *7*, 1700770.

37. Du, X., Heumueller, T., Gruber, W., Classen, A., Unruh, T., Li, N., and Brabec, C.J. (2019). Efficient Polymer Solar Cells Based on Non-fullerene Acceptors with Potential Device Lifetime Approaching 10 Years. Joule *3*, 215–226.

38. Yang, Y., Zhang, Z.G., Bin, H., Chen, S., Gao, L., Xue, L., Yang, C., and Li, Y. (2016). Side-Chain Isomerization on an n-type Organic Semiconductor ITIC Acceptor Makes 11.77% High Efficiency Polymer Solar Cells. J. Am. Chem. Soc. *138*, 15011–15018.

39. Baran, D., Gasparini, N., Wadsworth, A., Tan, C.H., Wehbe, N., Song, X., Hamid, Z., Zhang, W., Neophytou, M., Kirchartz, T., et al. (2018). Robust nonfullerene solar cells approaching unity external quantum efficiency enabled by suppression of geminate recombination. Nat. Commun. *9*, 2059.

40. Li, S., Ye, L., Zhao, W., Yan, H., Yang, B., Liu, D., Li, W., Ade, H., and Hou, J. (2018). A Wide Band Gap Polymer with a Deep Highest Occupied Molecular Orbital Level Enables 14.2% Efficiency in Polymer Solar Cells. J. Am. Chem. Soc. *140*, 7159–7167.

41. Hu, L., Liu, Y., Mao, L., Xiong, S., Sun, L., Zhao, N., Qin, F., Jiang, Y., and Zhou, Y. (2018). Chemical reaction between an ITIC electron acceptor and an amine-containing interfacial layer in non-fullerene solar cells. J. Mater. Chem. A Mater. Energy Sustain. *6*, 2273–2278.

42. Zhu, X., Hu, L., Wang, W., Jiang, X., Hu, L., and Zhou, Y. (2019). Reversible Chemical Reactivity of Non-Fullerene Acceptors for Organic Solar Cells under Acidic and Basic Environment. ACS Appl. Energy Mater. *2*, 7602–7608.

43. Du, X., Heumueller, T., Gruber, W., Almora, O., Classen, A., Qu, J., He, F., Unruh, T., Li, N., and Brabec, C.J. (2020). Unraveling the Microstructure-Related Device Stability for Polymer Solar Cells Based on Nonfullerene Small-Molecular Acceptors. Adv. Mater. *32*, e1908305.

**Cell Reports
Physical Science**
Article

**CellPress**
OPEN ACCESS

44. Zhang, S., Ye, L., Zhao, W., Liu, D., Yao, H., and Hou, J. (2014). Side Chain Selection for Designing Highly Efficient Photovoltaic Polymers with 2D-Conjugated Structure. Macromolecules 47, 4653–4659.

45. Liu, Y., Zhao, J., Li, Z., Mu, C., Ma, W., Hu, H., Jiang, K., Lin, H., Ade, H., and Yan, H. (2014). Aggregation and morphology control enables multiple cases of high-efficiency polymer solar cells. Nat. Commun. 5, 5293.

46. Zhao, W., Qian, D., Zhang, S., Li, S., Inganäs, O., Gao, F., and Hou, J. (2016). Fullerene-Free Polymer Solar Cells with over 11% Efficiency and Excellent Thermal Stability. Adv. Mater. 28, 4734–4739.

47. Xin, J., Meng, X., Xu, X., Zhu, Q., Naveed, H.B., and Ma, W. (2019). Cold Crystallization Temperature Correlated Phase Separation, Performance, and Stability of Polymer Solar Cells. Matter 1, 1316–1330.

48. Tournebize, A., Rivaton, A., Peisert, H., and Chassé, T. (2015). The Crucial Role of Confined Residual Additives on the Photostability of P3HT. PCBM Active Layers. J. Phys. Chem. C 119, 9142–9148.

49. Tremolet de Villers, B.J., O'Hara, K.A., Ostrowski, D.P., Biddle, P.H., Shaheen, S.E., Chabinyc, M.L., Olson, D.C., and Kopidakis, N. (2016). Removal of Residual Diiodooctane Improves Photostability of High-Performance Organic Solar Cell Polymers. Chem. Mater. 28, 876–884.

50. Ye, L., Jing, Y., Guo, X., Sun, H., Zhang, S., Zhang, M., Huo, L., and Hou, J. (2013). Remove the Residual Additives toward Enhanced Efficiency with Higher Reproducibility in Polymer Solar Cells. J. Phys. Chem. C 117, 14920–14928.

51. Kim, W., Kim, J.K., Kim, E., Ahn, T.K., Wang, D.H., and Park, J.H. (2015). Conflicted Effects of a Solvent Additive on PTB7:PC 71 BM Bulk Heterojunction Solar Cells. J. Phys. Chem. C 119, 5954–5961.

52. Wu, J., Luke, J., Lee, H.K.H., Shakya Tuladhar, P., Cha, H., Jang, S.-Y., Tsoi, W.C., Heeney, M., Kang, H., Lee, K., et al. (2019). Tail state limited photocurrent collection of thick photoactive layers in organic solar cells. Nat. Commun. 10, 5159.

53. Wu, J., Lee, J., Chin, Y.-C., Yao, H., Cha, H., Luke, J., Hou, J., Kim, J.-S., and Durrant, J.R. (2020). Exceptionally low charge trapping enables highly efficient organic bulk heterojunction solar cells. Energy Environ. Sci. 13, 2422–2430.

54. Shuttle, C.G., Hamilton, R., Nelson, J., O'Regan, B.C., and Durrant, J.R. (2010). Measurement of Charge-Density Dependence of Carrier Mobility in an Organic Semiconductor Blend. Adv. Funct. Mater. 20, 698–702.

55. Chambon, S., Rivaton, A., Gardette, J.-L., and Firon, M. (2007). Photo- and thermal

degradation of MDMO-PPV:PCBM blends. Sol. Energy Mater. Sol. Cells 91, 394–398.

56. Chambon, S., Rivaton, A., Gardette, J.-L., and Firon, M. (2008). Durability of MDMO-PPV and MDMO-PPV: PCBM blends under illumination in the absence of oxygen. Sol. Energy Mater. Sol. Cells 92, 785–792.

57. Wood, S., Hollis, J.R., and Kim, J.-S. (2017). Raman spectroscopy as an advanced structural nanoprobe for conjugated molecular semiconductors. J. Phys. D Appl. Phys. 50, 073001.

58. Razzell-Hollis, J., Limbu, S., and Kim, J.-S. (2016). Spectroscopic Investigations of Three-Phase Morphology Evolution in Polymer: Fullerene Solar Cell Blends. J. Phys. Chem. C 120, 10806–10814.

59. Limbu, S., Pont, S., Doust, A.B., Kwon, S., Fuller, P., Tan, E., Durrant, J.R., and Kim, J. (2019). Impact of Initial Bulk-Heterojunction Morphology on Operational Stability of Polymer:Fullerene Photovoltaic Cells. Adv. Mater. Interfaces 6, 1801763.

60. Drees, M., Hoppe, H., Winder, C., Neugebauer, H., Sariciftci, N.S., Schwinger, W., Schäffler, F., Topf, C., Scharber, M.C., Zhu, Z., et al. (2005). Stabilization of the nanomorphology of polymer–fullerene "bulk heterojunction" blends using a novel polymerizable fullerene derivative. J. Mater. Chem. 15, 5158.

61. Perea, J.D., Langner, S., Salvador, M., Sanchez-Lengeling, B., Li, N., Zhang, C., Jarvas, G., Kontos, J., Dallos, A., Aspuru-Guzik, A., et al. (2017). Introducing a New Potential Figure of Merit for Evaluating Microstructure Stability in Photovoltaic Polymer-Fullerene Blends. J. Phys. Chem. C 121, 18153–18161.

62. Ye, L., Collins, B.A., Jiao, X., Zhao, J., Yan, H., and Ade, H. (2018). Miscibility-Function Relations in Organic Solar Cells: Significance of Optimal Miscibility in Relation to Percolation. Adv. Energy Mater. 8, 1703058.

63. Ghasemi, M., Hu, H., Peng, Z., Rech, J.J., Angunawela, I., Carpenter, J.H., Stuard, S.J., Wadsworth, A., McCulloch, I., You, W., et al. (2019). Delineation of Thermodynamic and Kinetic Factors that Control Stability in Non-fullerene Organic Solar Cells. Joule 3, 1328–1348.

64. Zhu, Y., Gadisa, A., Peng, Z., Ghasemi, M., Ye, L., Xu, Z., Zhao, S., and Ade, H. (2019). Rational Strategy to Stabilize an Unstable High-Efficiency Binary Nonfullerene Organic Solar Cells with a Third Component. Adv. Energy Mater. 9, 1900376.

65. Aldrich, T.J., Matta, M., Zhu, W., Swick, S.M., Stern, C.L., Schatz, G.C., Facchetti, A., Melkonyan, F.S., and Marks, T.J. (2019). Fluorination Effects on Indacenodithienothiophene Acceptor Packing and Electronic Structure, End-Group

Redistribution, and Solar Cell Photovoltaic Response. J. Am. Chem. Soc. 141, 3274–3287.

66. Bristow, H., Thorley, K.J., White, A.J.P., Wadsworth, A., Babics, M., Hamid, Z., Zhang, W., Paterson, A.F., Kosco, J., Panidi, J., et al. (2019). Impact of Nonfullerene Acceptor Side Chain Variation on Transistor Mobility. Adv. Electron. Mater. 5, 1900344.

67. Han, G., Guo, Y., Song, X., Wang, Y., and Yi, Y. (2017). Terminal π-π stacking determines three-dimensional molecular packing and isotropic charge transport in an A-π-A electron acceptor for non-fullerene organic solar cells. J. Mater. Chem. C Mater. Opt. Electron. Devices 5, 4852–4857.

68. Mai, J., Xiao, Y., Zhou, G., Wang, J., Zhu, J., Zhao, N., Zhan, X., and Lu, X. (2018). Hidden Structure Ordering Along Backbone of Fused-Ring Electron Acceptors Enhanced by Ternary Bulk Heterojunction. Adv. Mater. 30, e1802888.

69. Collado-Fregoso, E., Boufflet, P., Fei, Z., Gann, E., Ashraf, S., Li, Z., McNeill, C.R., Durrant, J.R., and Heeney, M. (2015). Increased Exciton Dipole Moment Translates into Charge-Transfer Excitons in Thiophene-Fluorinated Low-Bandgap Polymers for Organic Photovoltaic Applications. Chem. Mater. 27, 7934–7944.

70. Frisch, M.J., Trucks, G.W., Schlegel, H.B., Scuseria, G.E., Robb, M.A., Cheeseman, J.R., Scalmani, G., Barone, V., Mennucci, B., Petersson, G.A., et al. (2009). Gaussian 09, Revision A.1.

71. Becke, A.D. (1993). Density-functional thermochemistry. III. The role of exact exchange. J. Chem. Phys. 98, 5648–5652.

72. Petersson, G.A., Bennett, A., Tensfeldt, T.G., Al-Laham, M.A., Shirley, W.A., and Mantzaris, J. (1988). A complete basis set model chemistry. I. The total energies of closed-shell atoms and hydrides of the first-row elements. J. Chem. Phys. 89, 2193–2218.

73. Petersson, G.A., and Al-Laham, M.A. (1991). A complete basis set model chemistry. II. Open-shell systems and the total energies of the first-row atoms. J. Chem. Phys. 94, 6081–6090.

74. Stephens, P.J., Devlin, F.J., Chabalowski, C.F., and Frisch, M.J. (1994). Ab Initio Calculation of Vibrational Absorption and Circular Dichroism Spectra Using Density Functional Force Fields. J. Phys. Chem. 98, 11623–11627.

75. Laury, M.L., Carlson, M.J., and Wilson, A.K. (2012). Vibrational frequency scale factors for density functional theory and the polarization consistent basis sets. J. Comput. Chem. 33, 2380–2387.

76. Besler, B.H., Merz, K.M., and Kollman, P.A. (1990). Atomic charges derived from semiempirical methods. J. Comput. Chem. 11, 431–439.